Quantifying Memory Effects in RF Power Amplifiers

Hyunchul Ku, *Student Member, IEEE*, Michael D. McKinley, *Member, IEEE*, and J. Stevenson Kenney, *Senior Member, IEEE*

***Abstract*—This paper proposes a system-level behavioral model for RF power amplifiers (PAs), which exhibit memory effects, that is based on the parallel Wiener system. The model extraction is performed using two-tone intermodulation distortion (IMD) measurements with different tone frequency spacings and power levels. It is found that by using such a model, more accurate adjacent-channel power-ratio levels may be predicted for high PAs close to the carrier frequency. This is validated using IS-95B CDMA signals on a low-power (0.5 W) class-AB PA, and on a high-power (45 W) class-B PA. The model also provides a means to quantify memory effects in terms of a figure-of-merit that calculates the relative contribution to the IMD of the memoryless and memory portion of the PA nonlinearity. This figure-of-merit is useful in providing an estimate of the amount of correction that a memoryless predistortion system may have on PAs that exhibit memory effects.**

***Index Terms*—Behavioral model, intermodulation distortion (IMD), memory effects, nonlinearities, power amplifier (PA), predistortion.**

I. Introduction

In WIRELESS communications, the transmitter power amplifier (PA) introduces nonlinearities when it operates near maximum output power. In system-level simulation, behavioral models are often employed to model the PA nonlinearities. These measurement-based empirical models provide a computationally efficient means to relate the input complex envelope to the output complex envelope without resorting to a physical level analysis of the PAs. Behavioral models for PAs can be classified into three categories depending on the existence of memory effects [1]–[3]: memoryless nonlinear systems, quasi-memoryless nonlinear systems, and nonlinear systems with memory. For the memoryless nonlinear system, the PA block is represented by the narrow-band AM/AM transfer function. For the quasi-memoryless nonlinear system, with memory time constants on the order of the period of the RF carrier, the PA block is often represented by AM/AM and AM/PM functions. Usually, AM/AM and AM/PM are measured by sweeping the power of a single tone in the center frequency of the passband of the RF PA. For a nonlinear system with long-term memory effects, on the order of the period of the envelope signal, the system response depends not only on the input envelope amplitude, but also its frequency. An alternate view is that the AM/AM and AM/PM functions appear to change as a function of past input levels. Such effects may arise in high power amplifiers (HPAs) from thermal effects, as well as long time constants in dc-bias networks. In [4], it was shown that an HPA with memory effects exhibits two-tone intermodulation distortion (IMD) that depends on the tone spacing. It is also shown in [4] that the application of a memoryless baseband predistortion algorithm gives significant improvement in adjacent channel power ratio (ACPR) to a 0.5-W handset low power amplifier (LPA). However, the same algorithm cannot significantly improve the nonlinearity of 45-W base-station HPA, which is shown to exhibit strong memory effects. Since predistortion methods depend heavily on the accuracy of the PA model, memoryless AM/AM and AM/PM are not sufficient to describe HPAs with memory effects.

A nonlinear system with memory can be represented by Volterra series, which are characterized by Volterra kernels [3]. However, the computation of the Volterra kernels for a nonlinear system is often difficult and time consuming for strongly nonlinear devices. In many applications that involve modeling of nonlinear systems, it is convenient to employ a simpler model. The Wiener model, which is cascade connection of linear time invariant (LTI) system and memoryless nonlinear system, has been used to model nonlinear PAs with memory [1], [5]–[8]. The Wiener model that is frequency-dependent memoryless nonlinear model yields identical shape, but only creates a shift with reference AM/AM and AM/PM curves [9].

In this paper, we propose a more accurate model based on the parallel Wiener model developed by Schetzen [3]. The first branch is set to a memoryless AM/AM and AM/PM model derived from single-tone measurements. The complex envelope transfer function is used to describe the AM/AM and AM/PM functions. Using two-tone signals, AM/AM and AM/PM curves are extracted for each envelope frequency by measuring IMD products. The derivation of the AM/AM and AM/PM complex function from two-tone measurement is proposed in Section II. The error between the memoryless model in the first branch and the measured data from two-tone is modeled by adding the cascade of the LTI system and the nonlinear function in parallel. In this way, long time constant memory effects may be modeled with a long-delay LTI system in a parallel branch. The modeling of a PA with memory effects is described in Section III. For the experimental validation, a 0.5-W LPA and 45-W HPA are modeled with the proposed method in Section IV. The derived model is simulated and compared with the measured results. Lastly, the extracted models are exercised to predict the level of distortion produced by the memoryless portion, and compared to that produced by the branches that model memory effects. This analysis provides a means for quantifying how strong the memory effects

Manuscript received April 5, 2002; revised August 26, 2002. This work was supported in part by the Yamacraw Design Center, an economic development project supported by the State of Georgia, and by Danam USA, San Jose, CA.

The authors are with the School of Electrical and Computer Engineering, Georgia Institute of Technology, Atlanta, GA 30332 USA (e-mail: gte661q@prism.gatech.edu).

Digital Object Identifier 10.1109/TMTT.2002.805196

are in a particular amplifier. Furthermore, noting that a memoryless predistortion algorithm is unable to remove the distortion produced by the memory terms, the effectiveness of such an algorithm on a particular PA may be estimated. Such estimates are calculated, and compared to previously reported measured results.

II. AM/AM, AM/PM, and Two-Tone Response

A bandpass input signal of a PA can be represented as

$$v(t) = \mathrm{Re}\{g(t)e^{j\omega_c t}\} = r(t)\cos\big(\omega_c t + \theta(t)\big) \tag{1}$$

where $g(t)$ is the input complex envelope signal, ω_c is the carrier center frequency, $r(t)$ is the amplitude of $g(t)$, and $\theta(t)$ is the phase of $g(t)$.

The nonlinear device such as a PA is usually represented by power series of the input signal. For the output of the fundamental zone bandpass filter, all even-order terms are filtered out, and the fundamental zone output of $v(t)^m$ is zero for even m. For odd-order powers with $m = 2k-1$ ($k = 1, 2, 3, \ldots$), the fundamental zone output of $v(t)^m$ is

$$v_{2k-1}(t) = \mathrm{Re}\left\{\frac{1}{4^{k-1}}\binom{2k-1}{k}|g(t)|^{2(k-1)}\,g(t)e^{j\omega_c t}\right\}. \tag{2}$$

Considering amplitude and phase change on each complex envelope of $v_{2k-1}(t)$, the bandpass output signal of the PA $w(t)$, which consists of $(2n-1)$th-order power series, can be described as follows:

$$\begin{aligned} w(t) &= \mathrm{Re}\left\{f(t)e^{j\omega_c t}\right\} \\ &= \mathrm{Re}\left\{\sum_{k=1}^{n} c_{2k-1}\frac{1}{4^{k-1}}\binom{2k-1}{k}|g(t)|^{2(k-1)}\,g(t)e^{j\omega_c t}\right\} \end{aligned} \tag{3}$$

where c_{2k-1} is a complex coefficient.

The output complex envelope $f(t)$ can be acquired as follows [10]:

$$f(t) = \sum_{k=1}^{n} a_{2k-1}|g(t)|^{2(k-1)}\,g(t) = \sum_{k=1}^{n} a_{2k-1}r(t)^{2k-1}e^{j\theta(t)} \tag{4}$$

where

$$a_{2k-1} = \frac{1}{4^{k-1}}\binom{2k-1}{k}c_{2k-1}. \tag{5}$$

In (4), the odd-order complex power series is defined as

$$F\big(r(t)\big) = \sum_{k=1}^{n} a_{2k-1}r(t)^{2k-1}. \tag{6}$$

AM/AM and AM/PM characteristic functions can then be jointly represented by $F(r(t))$ as follows:

$$w(t) = \Big|F\big(r(t)\big)\Big|\cos\Big(\omega_c t + \theta(t) + \angle F\big(r(t)\big)\Big) \tag{7}$$

where the AM/AM function is given by

$$\Big|F\big(r(t)\big)\Big| = \left[\sum_{k=1}^{n}\left(\sum_{i=1}^{k} a_{2i-1}a_{2k-2i+1}^{*}\right)r(t)^{2(2k-1)}\right]^{1/2} \tag{8}$$

and the AM/PM function is given by

$$\angle F\big(r(t)\big) = \arctan\left(\frac{\sum_{k=1}^{n}\mathrm{Im}\{a_{2k-1}\}r(t)^{2k-1}}{\sum_{k=1}^{n}\mathrm{Re}\{a_{2k-1}\}r(t)^{2k-1}}\right). \tag{9}$$

Using the complex envelope $f(t)$, AM/AM and AM/PM can be directly related with the two-tone response and vice versa. The two-tone input, which has magnitude $A/2$ and phase $\varphi(t)$ for each tone, with tone spacing $2\omega_m$, can be described as

$$\begin{aligned} v(t) &= \frac{A}{2}\Big[\cos\big((\omega_c-\omega_m)t+\varphi(t)\big)+\cos\big((\omega_c+\omega_m)t+\varphi(t)\big)\Big] \\ &= A\cos(\omega_m t)\cos\big(\omega_c t+\varphi(t)\big). \end{aligned} \tag{10}$$

For this two-tone input, the complex envelope $g(t)$ is $A\cos(\omega_m t)e^{j\varphi(t)}$. The output complex envelope $f(t)$ can then be acquired as follows [11]:

$$\begin{aligned} f(t) &= \sum_{k=1}^{n} a_{2k-1}A^{2k-1}\cos^{2k-1}(\omega_m t)e^{j\varphi(t)} \\ &= \sum_{k=1}^{n} d_{2k-1}\cos((2k-1)\omega_m t)e^{j\varphi(t)} \end{aligned} \tag{11}$$

where

$$d_{2k-1} = \sum_{i=k}^{n}\frac{1}{4^{i-1}}\binom{2i-1}{i-k}a_{2i-1}A^{2i-1}. \tag{12}$$

Thus, the PA output $\omega(t)$ for the two-tone input can be acquired using (3) and (11) as follows:

$$\begin{aligned} w(t) &= \mathrm{Re}\big\{f(t)e^{j\omega_c t}\big\} \\ &= \sum_{k=1}^{n}|d_{2k-1}|\cos\big((2k-1)\omega_m t\big)\cos\big(\omega_c t+\varphi(t)+\angle d_{2k-1}\big) \\ &= \sum_{k=1}^{n}\frac{|d_{2k-1}|}{2}\cos\big(\omega_c t\pm(2k-1)\omega_m t+\varphi(t)+\angle d_{2k-1}\big). \end{aligned} \tag{13}$$

Fig. 1 shows an illustration of the two-tone output resulting from (13). From (13), if the two-tone output characteristics are measured for input signals, which have different magnitudes $A_1, \ldots, A_l$ [12], the coefficients $d_{2k-1,1}, \ldots, d_{2k-1,l}$ ($k = 1, \ldots, n$) for each input signal can be acquired. The complex coefficient in (6) can be derived to minimize the error function

$$\min\sum_{k=1}^{n}\sum_{q=1}^{l}\lambda_k\kappa_q\left|d_{2k-1,q}-\sum_{i=k}^{n}\frac{1}{4^{i-1}}\binom{2i-1}{i-k}a_{2i-1}A_q^{2i-1}\right|^2 \tag{14}$$

where κ_q is the weighting factor depending on input power and λ_k is the weighting factor depending on the order of power series. These weighting factors can be determined to give a more

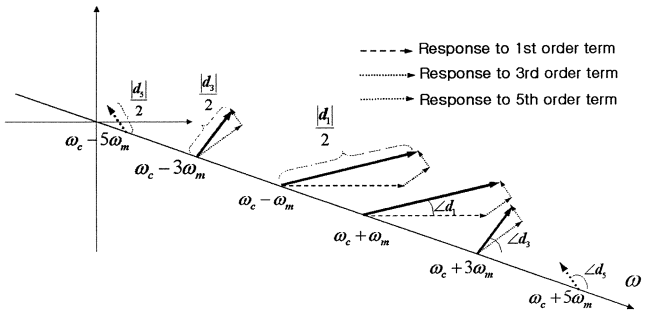

Fig. 1. Illustration of the two-tone output of a nonlinear device showing the relative phases of the IMD products.

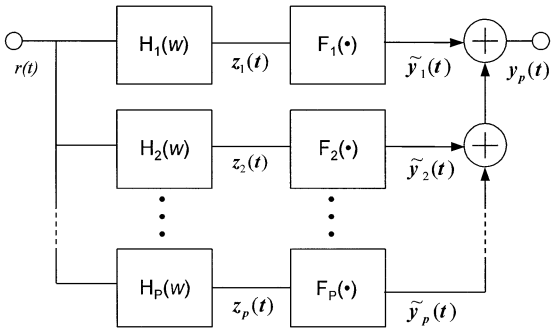

Fig. 2. PA model for a system with memory using the parallel Wiener model.

accurate model depending on the input signal statistics and PA characteristics.

III. Modeling of a PA That Exhibits Memory Effects

By sweeping envelope frequency ω_m, the frequency-dependent coefficient $a_{2k-1}(\omega_m)$ can be derived from two-tone measurements. Thus, the frequency-dependent complex power series $F(r,\omega_m)$, considering memory effects, can be described as

$$\begin{aligned} F(r,\omega_m) =& a_1(\omega_m)r + a_3(\omega_m)r^3 + \cdots + a_{2n-1}(\omega_m)r^{2n-1} \\ =& \sum_{k=1}^{n} a_{2k-1}(\omega_m)r^{2k-1}. \end{aligned} \tag{15}$$

Therefore, the output of a PA with memory effects is

$$w(t) = \left|F(r,\omega_m)\right| \cos\left(\omega_c t + \theta(t) + \angle F(r,\omega_m)\right). \tag{16}$$

The frequency-dependent complex polynomial in (15) can be realized by a parallel cascade structure of the LTI system connected in series with a memoryless nonlinear system, as shown in Fig. 2. In this model, the input signal $r(t)$ is $A\cos(\omega_m t)$, which is the two-tone envelope.

This model is simpler than the general Volterra system models, but has been shown to approximate memory effects well in other nonlinear systems [13]. The LTI system has the following characteristic function:

$$H_i(\omega) = \left|H_i(\omega)\right| e^{j\Omega_i(\omega)}. \tag{17}$$

$F_i(\cdot)$ is the complex polynomial with the coefficient $a_{2k-1,i}$ $(k = 1,\ldots,n, i = 1,\ldots,p)$. The output for the parallel Wiener system in Fig. 2 is

$$\begin{aligned} y_p(t) &= \sum_{i=1}^{p} \tilde{y}_i(t) \\ &= \sum_{i=1}^{p} F_i\big(z_i(t)\big) \\ &= \sum_{i=1}^{p}\sum_{k=1}^{n} a_{2k-1,i}\Big(A\left|H_i(\omega_m)\right| \cos\big(\omega_m t + \Omega_i(\omega_m)\big)\Big)^{2k-1} \end{aligned} \tag{18}$$

where p is the number of parallel branches, $z_i(t)$ is the output for the LTI system of the ith branch, and $\tilde{y}_i(t)$ is the output for the nonlinear system of the ith branch. In (18), $a_{2k-1,i}$ and $H_i(\omega_m)$ can be acquired to minimize mean square error $\overline{\varepsilon_i^2}$, where

$$\begin{aligned} \varepsilon_i =& F(r(t),\omega_m) - y_i(t) \\ =& F(r(t),\omega_m) - \sum_{s=1}^{i} \tilde{y}_s(t), \qquad i = 1,\ldots,p. \end{aligned} \tag{19}$$

The mean square error $\overline{\varepsilon_i^2}$ can be expressed in a recursive form

$$\overline{\varepsilon_i^2} = \overline{\left(\varepsilon_{i-1} - \tilde{y}_i\right)^2} = \overline{\varepsilon_{i-1}^2} + \overline{\tilde{y}_i^2} - 2\mathrm{Re}\{\overline{\varepsilon_{i-1}\tilde{y}_i^*}\}. \tag{20}$$

A parameter-estimation technique for the nonlinear parallel system has been developed [14], [15]. The parameter identification procedure for the parallel Wiener PA model can be outlined as follows. The first branch of the system is set to be the memoryless model. Thus, the linear system $H_1(\omega_m)$ has time response $h_1(t) = \delta(t)$ and the nonlinear system $F_1(\cdot)$ has AM/AM and AM/PM response derived from single-tone measurements. The linear system $H_i(\omega_m)$, $(i = 2,\ldots,p)$ can be acquired using the cross-correlation function of the input $r(t)$ and the error ε_{i-1}. The coefficients $a_{2k-1,i}$ $(k = 1,\ldots,n)$ of $F_i(\cdot)$ $(i = 2,\ldots,p)$ are determined to minimize the mean square error $\overline{\varepsilon_i^2}$ in (20) for the input $z_i(t)$. The branches are added until $\overline{\varepsilon_i^2}$ is less than some threshold value.

For simplicity, Ω_i $(i = 1,\ldots,p)$ is set to zero, and then the error in (19) can be represented by

$$\begin{aligned} \varepsilon_i = & \sum_{k=1}^{n} A^{2k-1}\cos^{2k-1}(\omega_m t) \\ & \cdot\left[a_{2k-1}(\omega_m) - \sum_{s=1}^{i} a_{2k-1,s}\left|H_s(\omega_m)\right|^{2k-1}\right]. \end{aligned} \tag{21}$$

The difference between the frequency-dependent coefficient $a_{2k-1}(\omega_m)$ and the memoryless branch coefficient $a_{2k-1,1}$ is defined as

$$\tilde{a}_{2k-1}(\omega_m) = a_{2k-1}(\omega_m) - a_{2k-1,1}. \tag{22}$$

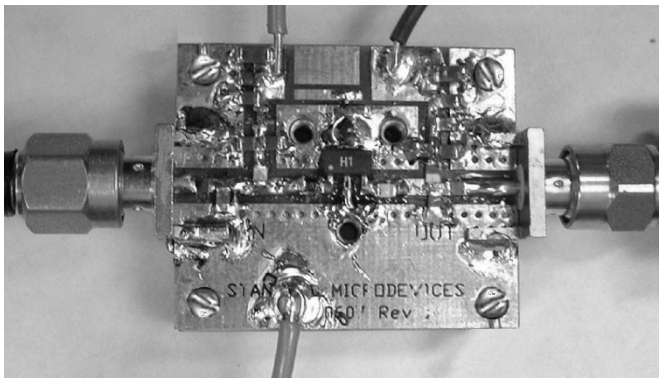

Fig. 3. 0.5-W GaAs HFET class-AB linear PA used in this study.

To quantify the frequency dependence of each coefficient, $\hat{a}_{2k-1}$ is defined as

$$\hat{a}_{2k-1} = \left(\frac{1}{\omega_2 - \omega_1} \int_{\omega_1}^{\omega_2} \left| \frac{\tilde{a}_{2k-1}(\omega_m)}{a_{2k-1,1}} \right|^2 d\omega_m \right)^{1/2} \quad (23)$$

where ω_1 is the lower frequency, and ω_2 is the upper frequency. Equation (23) establishes a figure-of-merit that quantifies the contribution of the memory effect terms relative to the memoryless terms in the frequency zones affected by IMD of order $2k-1$. Such a figure-of-merit may be used to quantify the relative strength of memory effects between amplifiers: high values of $\hat{a}_{2k-1}$ indicate strong contributions from memory effect terms.

IV. Experimental Validation

For the experimental validation, two-tone output was measured versus tone-spacing (2.5–1300 kHz) and input power around the P1 dB for the Sirenza Microdevices 0.5-W handset PA, shown in Fig. 3, and the Ericsson 45-W base-station PA, shown in Fig. 4. The LPA is an AlGaAs/GaAs HFET class-AB PA. The HPA is silicon bipolar junction transistor (BJT)-based class-B PA that has the operating frequency at 885 MHz. The Ericsson PA was designed for use with constant envelope (AMPS) signals, hence, it exhibits strong memory effects for amplitude modulated signals. In the unit under test, it was found that AM/PM effects had a negligible effect on the close-in ACPR. Thus, to simplify the extraction procedure, AM/PM effects were ignored. The measured third-order intermodulation distortion (IMD3) and fifth-order intermodulation distortion (IMD5) amplitude responses of a 0.5-W LPA for several tone spacings are plotted in Figs. 5 and 6. The measured IMD3 and IMD5 of a 45-W HPA are plotted in Figs. 7 and 8. In Figs. 5 and 6, the variation of IMD3 and IMD5 is small (less than a few decibels). In contrast, as shown in Figs. 7 and 8, the Ericsson 45-W class-B PA IMD versus frequency spacing and output power response is quite variable, which results from strong memory effects. Using the fifth-order complex envelope function, the coefficients are derived by changing the envelope frequency. To compare the variation of coefficients for the LPA and HPA, $\tilde{a}_{2k-1}(\omega_m)/a_{2k-1,1}$ ($k = 1,2,3$) are plotted in Fig. 9. The coefficient functions versus envelope frequency for the 0.5-W LPAare almost the same as $a_{2k-1,1}$ ($k = 1,2,3$) . For the 45-W HPA, $a_1(\omega_m)$ is almost the same as the $a_{1,1}$, but $a_3(\omega_m)$ and $a_5(\omega_m)$ show much variation compared to $a_{3,1}$ and $a_{5,1}$.

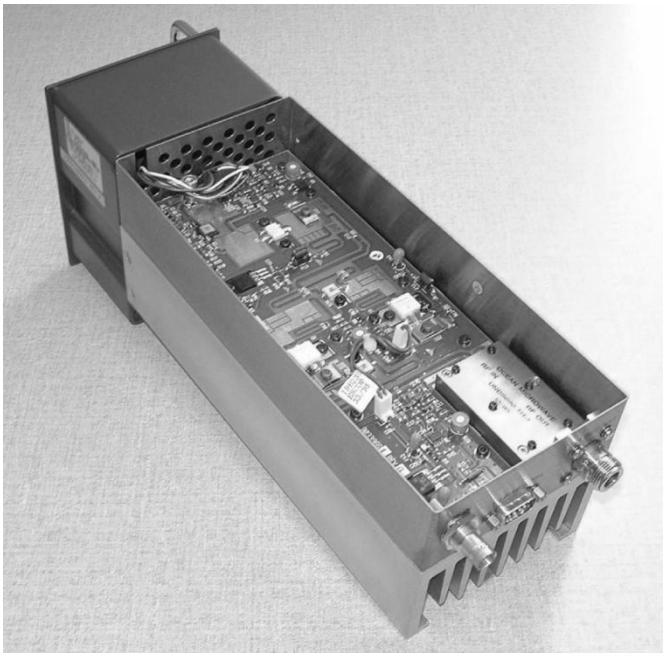

Fig. 4. 45-W Si-bipolar class-B base station HPA used in this study.

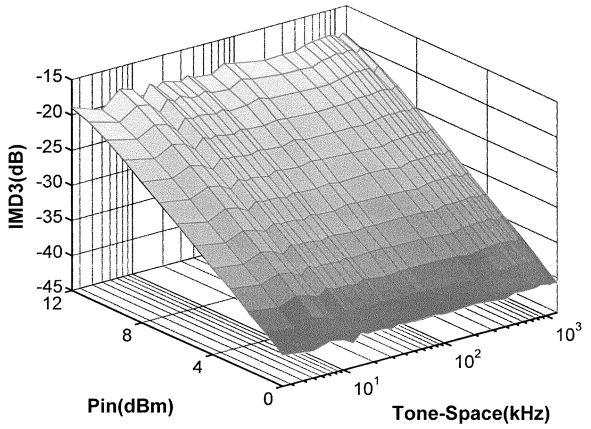

Fig. 5. Measured IMD3 versus tone spacing and power input for the 0.5-W LPA.

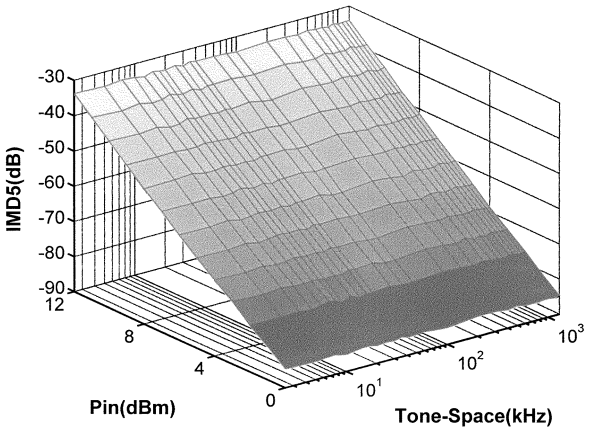

Fig. 6. Measured IMD5 versus tone spacing and power input for the 0.5-W LPA.

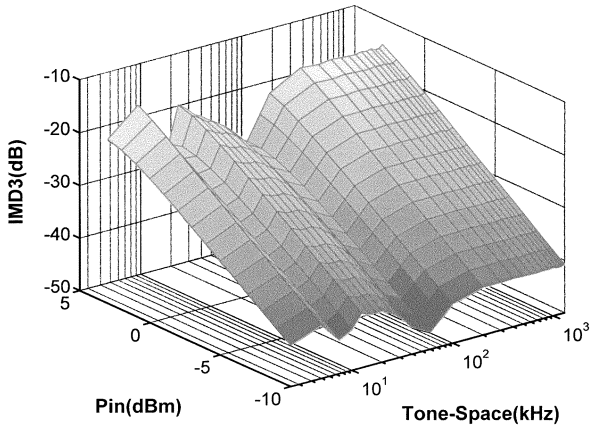

Fig. 7. Measured IMD3 versus tone spacing and power input for the 45-W HPA.

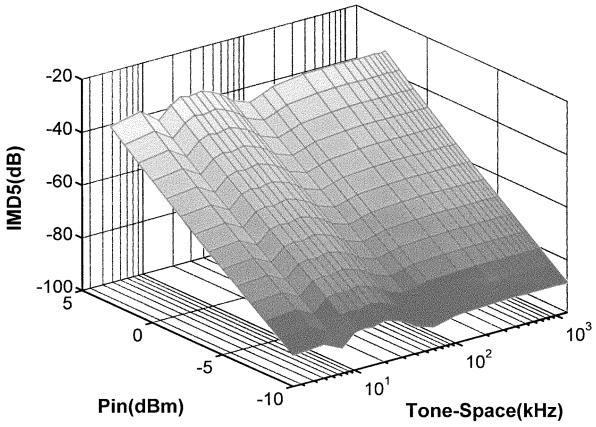

Fig. 8. Measured IMD5 versus tone spacing and power input for the 45-W HPA.

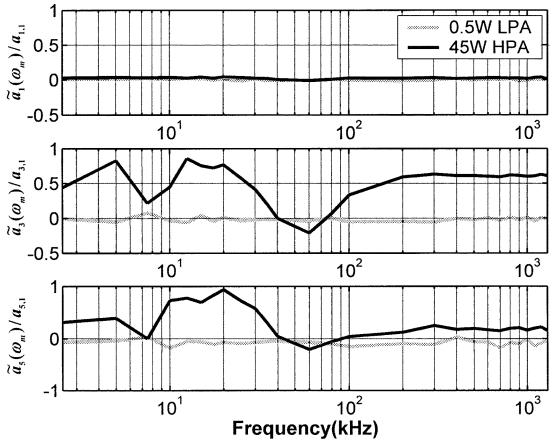

Fig. 9. Comparison of the error between the frequency-dependent coefficient $a_{2k-1}(\omega_m)$ and the memoryless branch coefficient $a_{2k-1,1}$ normalized to $a_{2k-1,1}$ for the LPA and HPA.

To model these PAs, the parallel Wiener model was used, which consists of four parallel branches. The first branch is the memoryless part, and the sum of the additional branches (second, third, and fourth branch) is the part due to the memory effects. The infinite impulse response (IIR) filters are used for the LTI systems. The spectral regrowth was predicted for an IS-95B CDMA signal, and compared to the measured results

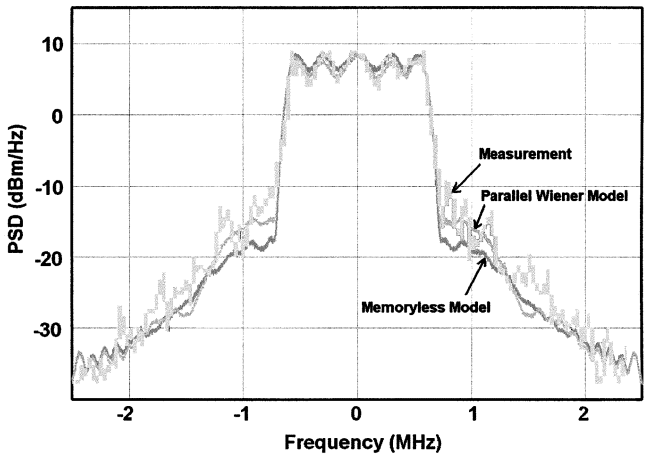

Fig. 10. Predicted and measured spectral regrowth for an IS-95B CDMA signal (HPA).

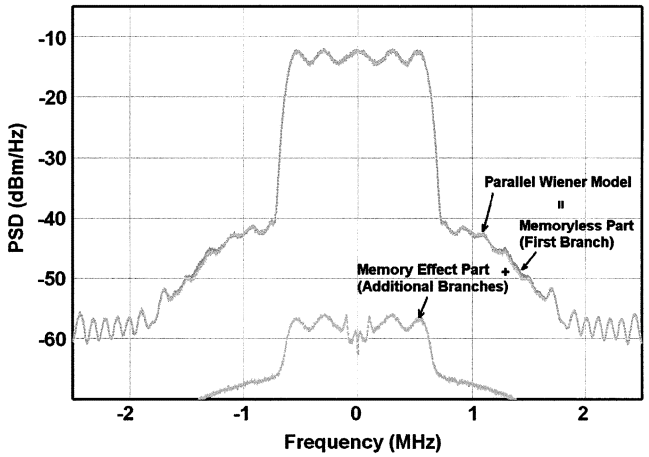

Fig. 11. Predicted spectral regrowth for an IS-95B CDMA signal using the parallel Wiener model (LPA).

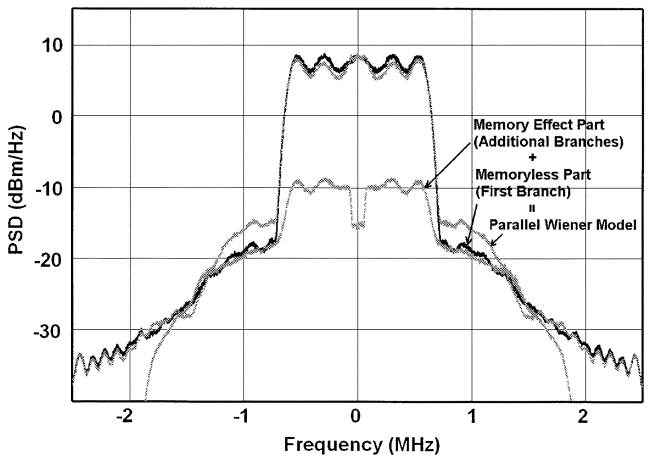

Fig. 12. Predicted spectral regrowth for an IS-95B CDMA signal using the parallel Wiener model (HPA).

in Fig. 10 for the HPA. The output from the parallel Wiener model is also compared to a conventional memoryless model. It is seen that the parallel Wiener model, which was acquired from two-tone measurements, gives more accurate spectral regrowth results than the AM/AM model by as much as 4 dB for close-in

TABLE I
NORMALIZED rms DIFFERENCE BETWEEN THE FREQUENCY-DEPENDENT COEFFICIENTS $a_{2k-1}(\omega_m)$ AND THE MEMORYLESS COEFFICIENTS $a_{2k-1,1}$ FOR THE LPA AND HPA, AS CALCULATED FROM (23), AS MEASURED IN DECIBELS

	$20log\|\hat{a}_1\|$	$20log\|\hat{a}_3\|$	$20log\|\hat{a}_5\|$
LPA	-38.8	-30.1	-21.1
HPA	-31.8	-5.09	-7.61

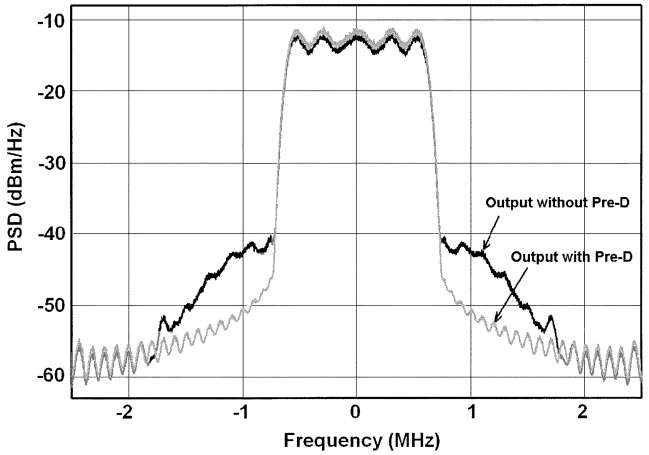

Fig. 13. Predicted spectral regrowth for an IS-95B CDMA signal using the parallel Wiener model and memoryless predistortion (LPA).

spectral regrowth. For the LPA, the spectral regrowths predicted by the memoryless model and parallel Wiener model are almost the same, as shown in Fig. 11.

To compare the amount of memory effects for the LPA and HPA in the parallel Wiener model, the spectral regrowths due to the memoryless part (the first branch) and the part of memory effects (the sum of additional branches) are simulated in Figs. 11 and 12. For the LPA, the contribution of the memory effect branches is over 25 dB below that of the memoryless part, an indication that this PA is virtually memoryless. For the HPA, the contribution of the memory effect branches is almost the same as that of the memoryless branch for the close-in ACPR. Equation (23) is calculated for the third- and fifth-order terms for both the LPA and HPA. These results are summarized in Table I. Equation (23) is validated as an estimate of the contribution of the memory effects to the total IMD response by noting that the values in Table I are close to the relative contributions for each IMD order, as shown in Figs. 11 and 12 for the LPA and HPA, respectively.

A memoryless predistortion linearizer is inserted between the parallel Wiener model and signal source, and spectral regrowth for the IS-95B CDMA signal is simulated for the LPA and HPA, as shown in Figs. 13 and 14, respectively. The predistortion algorithm is optimized to generate a signal predistorted with the inverse nonlinear characteristics of the memoryless part in the parallel Wiener model. It is seen that this predistortion linearizer reduces spectral regrowth for the LPA by approximately 10 dB. This result was validated by measurement in [4]. As seen in Fig. 14, since the contribution of the memory effect branches is large for the HPA, the improvement from using memoryless predistortion is negligible. The simulation results discussed above are validated by experimental results reported in [4] by Kenney *et al.*

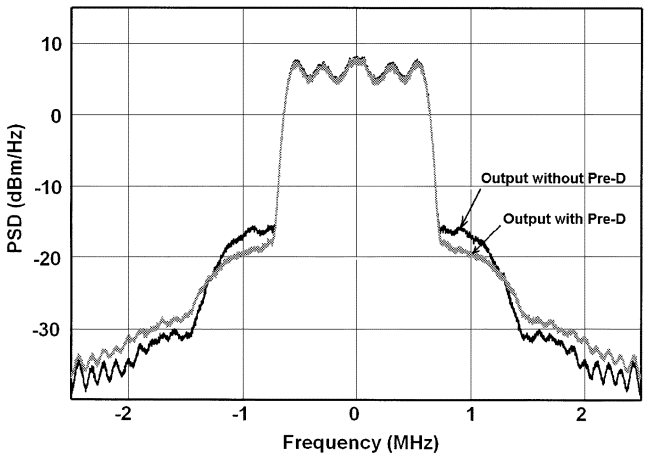

Fig. 14. Predicted spectral regrowth for an IS-95B CDMA signal using the parallel Wiener model and memoryless predistortion (HPA).

V. CONCLUSION

In this paper, we have proposed an accurate behavioral model for RF PAs that exhibit strong memory effects. Long-time constant memory effects are identified by measuring the variation in the output two-tone IMD versus tone spacing. This set of measurements maps out a two-dimensional transfer function that depends on the envelope frequency and amplitude of the input signal. The frequency-dependent transfer functions are then fit to the parallel Wiener model, which is a special case of the full Volterra series. Since long-time constant memory effects may be included in parallel branches, PA models using the parallel Wiener model can give a more accurate prediction for the output two-tone IMD amplitude and phase variation versus envelope frequency due to the memory effects. The model, which was extracted from two-tone measurements, was validated by comparing the predicted ACPR for an IS-95B CDMA signal and the measured result. It was seen that the model predicted the ACPR well. The model was also compared to a memoryless model derived from single-tone measurements. It was seen that the inclusion of memory effects afforded by the parallel Wiener model improved the accuracy of close-in ACPR prediction by as much as 4 dB. A figure-of-merit was developed that represents the relative contribution of memory effects to the total IMD at a particular order. The proposed model was also validated by comparing the predicted improvement by a memoryless predistortion algorithm to experimental results. Both the LPA and HPA cases were considered. Better than 10 dB of ACPR correction was seen when applying the predistortion algorithm to the LPA. In contrast, the memory effects present in the HPA substantially inhibited the improvement in the ACPR afforded by the memoryless predistortion algorithm. The simulated results are in good agreement with previously reported experimental results.

ACKNOWLEDGMENT

The authors wish to thank Ericsson USA Inc., Lynchburg, VA, and Sirenza Microdevices, Sunnyvale, CA, for donating the PAs used in this study. The authors also wish to thank W. Woo, a Ph.D. student at the Georgia Institute of Technology, Atlanta, Prof. G. T. Zhou, Georgia Institute of Technology, and two of her Ph.D. students, L. Ding and R. Raich, for their helpful comments in the development of this model.

REFERENCES

[1] T. Vuong and A. F. Guibord, "Modeling of nonlinear elements exhibiting frequency-dependent AM/AM and AM/PM transfer characteristics," *Can. Electr. Eng. J.*, vol. 9, no. 3, pp. 112–116, 1984.

[2] W. Bosch and G. Gatti, "Measurement and simulation of memory effects in predistortion linearizers," *IEEE Trans. Microwave Theory Tech.*, vol. 37, pp. 1885–1890, Dec. 1989.

[3] M. Schetzen, "Nonlinear system modeling based on the Wiener theory," *Proc. IEEE*, vol. 69, pp. 1557–1573, Dec. 1981.

[4] J. S. Kenney, W. Woo, L. Ding, R. Raich, H. Ku, and G. T. Zhou, "The impact of memory effects on predistortion linearization of RF power amplifiers," in *Proc. 8th Int. Microwave Opt. Technol. Symp.*, Montreal, QC, Canada, June 19–23, 2001, pp. 189–193.

[5] H. B. Poza, Z. A. Sarkozy, and H. L. Berger, "A wideband data link computer simulation model," in *Proc. IEEE Nat. Aerospace Electron. Conf.*, 1975, pp. 71–78.

[6] A. A. M. Saleh, "Frequency-independent and frequency-dependent nonlinear models of TWT amplifiers," *IEEE Trans. Commun.*, vol. COM-29, pp. 1715–1720, Nov. 1981.

[7] M. T. Abuelma, "Frequency-dependent nonlinear quadrature model for TWT amplifiers," *IEEE Trans. Commun.*, vol. COM-32, pp. 982–986, Aug. 1984.

[8] M. S. Muha, C. J. Clark, A. A. Moulthrop, and C. P. Silva, "Validation of power amplifier nonlinear block models," in *IEEE MTT-S Int. Microwave Symp. Dig.*, 1999, pp. 759–762.

[9] R. Blum and M. C. Jeruchim, "Modeling nonlinear amplifiers for communication simulations," in *IEEE Int. Commun. Conf.*, Boston, MA, 1989, pp. 1468–1472.

[10] K. G. Gard, H. M. Gutierrez, and M. B. Steer, "Characterization of spectral regrowth in microwave amplifiers based on the nonlinear transformation of a complex Gaussian processes," *IEEE Trans. Microwave Theory Tech.*, vol. 47, pp. 1059–1069, July 1999.

[11] S. Yi, S. Nam, S. Oh, and J. Han, "Predistortion of a CDMA output spectrum based on intermodulation products of two-tone test," *IEEE Trans. Microwave Theory Tech.*, vol. 49, pp. 938–946, May 2001.

[12] Y. Yang, J. Yi, J. Nam, B. Kim, and M. Park, "Measurement of two-tone transfer characteristics of high power amplifiers," *IEEE Trans. Microwave Theory Tech.*, vol. 49, pp. 568–571, Mar. 2001.

[13] V. J. Mathews and G. L. Sicuranza, *Polynomial Signal Processing*. New York: Wiley, 2000.

[14] M. J. Korenberg, "Parallel cascade identification and kernel estimation for nonlinear systems," *Ann. Biomed. Eng.*, vol. 19, pp. 429–455, May 1991.

[15] H. W. Chen, "Modeling and identification of parallel nonlinear systems: Structural classification and parameter estimation methods," *Proc. IEEE*, vol. 83, pp. 39–65, Jan 1995.

Hyunchul Ku (S'00) was born in Pusan, Korea, in 1972. He received the B.S. (*cum laude*) and M.S. degrees in electrical engineering from Seoul National University in Seoul, Korea, in 1995 and 1997 respectively, and is currently working toward the Ph.D. degree in electrical and computer engineering at the Georgia Institute of Technology, Atlanta.

From 1997 to 1999, he was a Member of Technical Staff with the Wireless Research Center, Korea Telecom, Seoul, Korea. His current research interests include behavioral modeling and characterization of RF devices, power-amplifier linearization, and statistical signal processing.

Michael D. McKinley (S'94–M'96) was born in Kodiak, AK, on June 17, 1970. He received the B.S. (*cum laude*) in physical science from Biola University, La Mirada, CA, in 1994, the B.S.E.E. degree (*magna cum laude*) from Gonzaga University, Spokane, WA, in 1995, the M.S.E.E. degree from Northeastern University, Boston, MA in 2001, and is currently working toward the Ph.D. degree in electrical engineering at the Georgia Institute of Technology, Atlanta.

During 1995, he was a Junior Engineer with the Itronix Corporation, Spokane, WA. From 1996 to 1998, he was a Hardware Design Engineer with the Intel Corporation, Hillsboro, OR. For most of 2000, he was an Engineering Intern with the RF Components Group, Raytheon, Andover, MA. His current research interests include the characterization and modeling of microwave power transistors and power-amplifier design.

Mr. McKinley is a student member of Tau Beta Pi. He was the recipient of the 1997 Intel Achievement Award for his work on high-speed motherboards.

J. Stevenson Kenney (S'84–M'85–SM'01) was born in St. Louis, MO, in 1962. He received the B.S.E.E. degree (with honors), M.S.E.E. degree, and Ph.D. degree in electrical engineering from the Georgia Institute of Technology, Atlanta, in 1985, 1990, and 1994, respectively.

In January 2000, he joined the faculty at the Georgia Institute of Technology, where he is currently an Associate Professor of electrical and computer engineering. He currently teaches and conducts research in the areas of power-amplifier linearization, smart antenna design, and RF integrated circuit (RFIC) design. He possesses over 14 years of industrial experience in wireless communications. He has held engineering and management positions with Electromagnetic Sciences, Scientific Atlanta, and Pacific Monolithics. Prior to rejoining the Georgia Institute of Technology, he was Director of Engineering with the Spectrian Corporation, Sunnyvale, CA. He has authored or coauthored over 40 technical papers, conference papers, and workshop presentations in the areas of acoustics, microelectronics, microwave design, and telecommunications.

Dr. Kenney has been an active member of the IEEE Microwave Theory and Techniques Society (IEEE MTT-S) for 16 years. He has served as an officer on the Santa Clara Valley chapter of the IEEE MTT-S from 1996 to 2000. He is currently serving his second term on the IEEE MTT-S Administrative Committee (AdCom), and was the treasurer for 2001 and 2002. He served on the IEEE MTT-S International Microwave Symposium (IMS) Steering Committee in 1993 and 1996. He has served on the Editorial Board for the IEEE TRANSACTIONS ON MICROWAVE THEORY AND TECHNIQUES AND THE IEEE MICROWAVE AND WIRELESS COMPONENTS LETTERS, and serves on the IEEE MTT-S IMS Technical Program Committee. He is currently co-chair of the RF Components Technical Interest Group of the National Electronics Manufacturing Initiative. He was the Technical Program Committee co-chair for the 2002 Radio and Wireless Conference (RAWCON).